



ELSEVIER

Available online at [www.sciencedirect.com](http://www.sciencedirect.com)

SCIENCE @ DIRECT®

Physica D 184 (2003) 21–28

PHYSICA D

[www.elsevier.com/locate/physd](http://www.elsevier.com/locate/physd)

# Nonextensivity in turbulence in rotating two-dimensional and three-dimensional flows

Charles N. Baroud\*, Harry L. Swinney

*Center for Nonlinear Dynamics and Department of Physics, The University of Texas at Austin, Austin, TX 78712, USA*

## Abstract

Our experiments on turbulent flow in a rotating annulus yield probability distribution functions (PDFs) for velocity increments  $\delta v(\ell)$ , where  $\ell$  is the separation between points. We fit these PDFs to a form derived for turbulent flows by Beck, who used the Tsallis nonextensive statistical mechanics formalism. For slow rotation rates, we find that the fit parameter  $q$  is 1.25 for small  $\ell$ . At large  $\ell$ ,  $q$  decreases to unity, the value corresponding to the usual Boltzmann–Gibbs statistics. These results agree with those previously measured in experiments on Couette–Taylor turbulence. However, with rapid rotation of the annulus, the turbulent flow becomes strongly two-dimensional (2D) rather than three-dimensional (3D), and we find  $q = 1.32 \pm 0.04$ , independent of  $\ell$ . This suggests that the coherent structures (vortices), which are a source of intermittency, are important at all length scales in the 2D case.

© 2003 Elsevier B.V. All rights reserved.

PACS: 47.27.–i; 92.10.Lq; 05.70.Ln

Keywords: Turbulence statistics; Nonextensive entropy; Anomalous scaling

## 1. Introduction

Two-dimensional (2D) turbulence was discussed by Kraichnan in 1967 with the caveat that it was *nowhere realized in nature* [1]. Since then, however, quasi-2D flows have been produced in laboratory experiments by using magnetic fields [2], stratification [3], or rotation [4]. These methods produce quasi-2D regimes that correspond to different limits on the Navier–Stokes equations; the relationship between these different limits and the true 2D case is not well understood.

For a rotating fluid, the 2D approximation improves as the rotation rate of the system is increased. We have studied the transition between three-dimensional (3D) and quasi-2D turbulence using a rotating annulus with a variable rotation rate [5,6]. At low rotation rates, the statistics of 3D turbulence were recovered: the probability distribution functions (PDFs) of velocity differences

$$\delta v(\ell) = v(x + \ell) - v(x) \quad (1)$$

displayed a strong dependence on the scale  $\ell$ ; for small  $\ell$ , the PDFs had power-law tails, and for large  $\ell$  the PDFs approached a Gaussian shape. At high rotation rates, the flow became essentially 2D and the resultant PDFs were self-similar, i.e., the shape was independent of  $\ell$  for length scales within the inertial range [4]. However, in contrast to results obtained in strati-

\* Corresponding author. Present address: Laboratoire d'Hydrodynamique (LadHyX), Ecole Polytechnique, 91128 Palaiseau, France.

E-mail addresses: [baroud@ladhyx.polytechnique.fr](mailto:baroud@ladhyx.polytechnique.fr) (C.N. Baroud), [swinney@chaos.ph.utexas.edu](mailto:swinney@chaos.ph.utexas.edu) (H.L. Swinney).

fied flow experiments [3], our PDFs for 2D turbulence exhibited a strong deviation from Gaussianity at all length scales. Strongly non-Gaussian PDFs are well established for 3D turbulence on small spatial scales (e.g., see Fig. 3 of [7]), but on large scales the PDFs become Gaussian. Extended tails have been found in numerous other situations (e.g., see [8–14]). Here we compare the 2D and 3D turbulent regimes by fitting the observed PDFs for velocity differences to a form derived by Beck [15] from the Tsallis nonextensive statistical mechanics formalism [16]. The functional form for the PDFs derived by Beck has been previously found to fit data for 3D turbulence for a wide range of length scales  $\ell$  in flow between concentric rotating cylinders (the Couette–Taylor system) [17] and flow between counter-rotating disks [18].

Section 2 describes our experiment and Section 3 summarizes Beck’s prediction for the velocity PDF for turbulent flow. Section 4 presents the analysis of our data in terms of this PDF. These results are discussed in Section 5.

## 2. Experimental apparatus and flow description

Our apparatus consists of a rotating annular tank filled with water [19]. The tank is covered with a flat

rigid lid, and the bottom is conical to approximate the beta effect, the variation of Coriolis force with latitude. The water is pumped in a closed circuit through two concentric rings of holes in the bottom of the tank. In the present experiments, fluid is pumped into the tank at a radius of 18.9 cm, and out of the tank at a radius of 35.1 cm. The net outward flux couples with the Coriolis force to generate an azimuthal counter-rotating jet. Measurements were made for two sets of control parameters: a quasi-2D turbulent flow was obtained with rotation rate  $\Omega = 11.0$  rad/s and pumping rate  $Q = 150$  cm<sup>3</sup>/s, and a 3D flow was obtained with  $\Omega = 1.57$  rad/s and  $Q = 450$  cm<sup>3</sup>/s.

The Reynolds numbers, based on the peak velocity  $U$  measured with hot film probes and a length scale  $L$  equal to the distance between the forcing rings, were 35,000 and 26,000 for the fast and slow rotation rates, respectively. A drawing of the apparatus and a discussion of the Reynolds numbers are given in Ref. [6].

The azimuthal component of the velocity was measured with hot film probes placed midway between the inner and outer walls of the annulus. The probes were mounted on the top lid and extended a distance of 1 cm into the fluid, well outside the thin Ekman boundary layer. The data sampling rate was 150 Hz (with a low-pass filter at 75 Hz) for 2 h long runs, giving a total of  $10^6$  points in each time series [5]. The

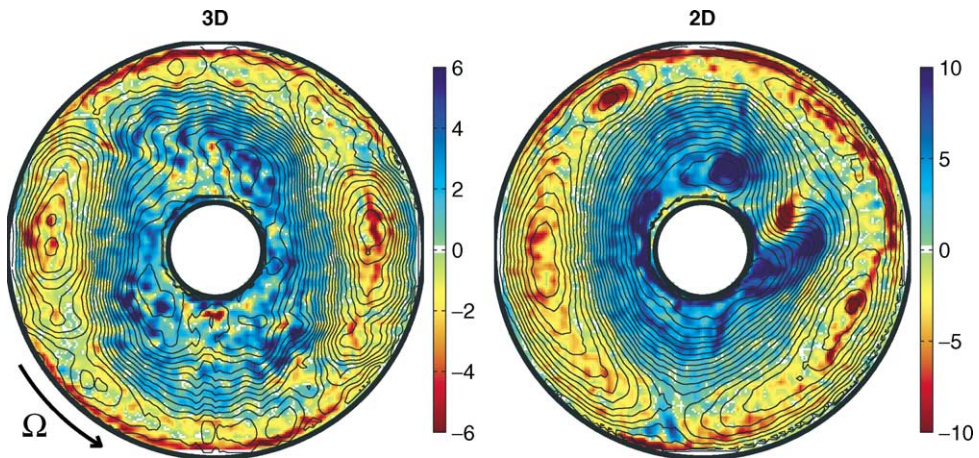


Fig. 1. Vorticity and streamfunction maps for the 3D and 2D flows, at  $\Omega = 1.57$  and  $11.0$  rad/s, respectively. The cyclonic (red center) and anti-cyclonic (blue center) vortices are advected clockwise by the mean anti-cyclonic jet, as the tank rotates counter-clockwise. The spacing of the streamline contours is  $12$  cm<sup>2</sup>/s for the 3D case and  $30$  cm<sup>2</sup>/s for the 2D case, and the color bars show the vorticity values (s<sup>-1</sup>).

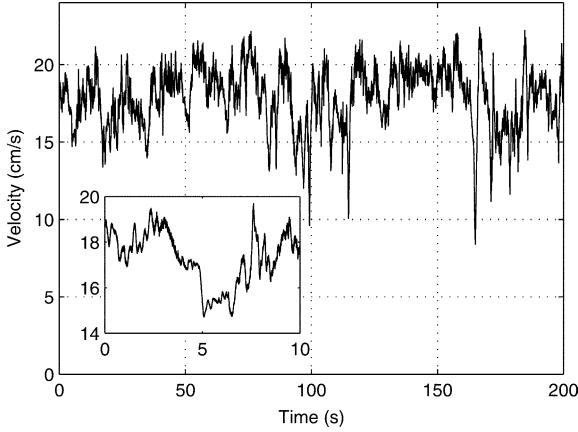


Fig. 2. Typical velocity time series measured at  $\Omega = 11.0$  rad/s and  $Q = 150$  cm<sup>3</sup>/s. The 10 s data segment shown in the inset illustrates the fine turbulent structure superposed on the large fluctuations in this 2D flow.

Taylor *frozen turbulence* hypothesis was used in the analysis, thus mapping the data from time to space.

In contrast to co-rotating jets which are strong and narrow, a counter-rotating jet is highly unstable and becomes turbulent even at low pumping flux  $Q$  [20]. The two-dimensionalization, however, is conducive to the formation of long-lived coherent vortices, which are advected clockwise by the mean flow (see Fig. 1). The velocity at which the vortices travel varies as they interact with the jet and with each other; same sign vortices merge, while those of opposite signs repel. Compact intense vortices also form in the recirculation regions of the large structures; these vortices have a strong effect on the motion of the mean flow. As the meandering jet sweeps past the probes, there is a switching between regions of high azimuthal velocity and regions where the flow is primarily in the radial direction. This switching, observed as a dip in the azimuthal velocity (Fig. 2), is an essential factor in the broadening of the tails of the PDFs (see Section IV.B of Ref. [5] and Section 2 of Ref. [6]).

### 3. Nonextensive entropy

The entropy for a nonequilibrium system can be nonextensive, which means that entropies for sub-

systems cannot be added to obtain the entropy for the whole system: if  $\mathcal{S}_q(A)$  and  $\mathcal{S}_q(B)$  are the entropies of two probabilistically independent systems, then  $\mathcal{S}_q(A+B) = \mathcal{S}_q(A) + \mathcal{S}_q(B) + (1-q)\mathcal{S}_q(A)\mathcal{S}_q(B)$ , where  $q-1$  is a measure of the degree of nonextensivity [21]. There is a very large literature on nonextensivity (<http://www.tsallis.cat.cbpf.br/TEMUCO.pdf>). We consider a particular form for the nonextensive entropy that has been proposed by Tsallis [16]:

$$\mathcal{S}_q = \frac{1}{q-1} \left( 1 - \sum_i p_i^q \right), \quad (2)$$

where  $p_i$  is the probability of the system being in a given state  $i$ . The Tsallis entropy reduces to the standard (Boltzmann–Gibbs) entropy,  $-\sum p_i \ln p_i$  in the limit  $q \rightarrow 1$ .

In our experiments we determine the probability  $p(\delta v(\ell))$  of a velocity difference  $\delta v(\ell)$  at length scale  $\ell$ , where  $\delta v$  is the longitudinal velocity difference (i.e., the velocity components are taken along the line of length  $\ell$ ). The goal of this work is to determine how values of the nonextensivity parameter  $q$  deduced from measurements of  $p(\delta v(\ell))$  depend on  $\ell$ , and to compare values of  $q$  obtained for the 3D and quasi-2D flows. Beck has used the Tsallis entropy (2) to derive the following form for  $p(\delta v)$ , assuming that the probability is normalized (the probabilities  $p_i$  add to unity) and satisfies a constraint on the total energy [15]:

$$p(\delta v) = \frac{1}{Z_q} [1 + \beta(q-1)\epsilon(\delta v)]^{-1/(q-1)}, \quad (3)$$

$$\beta = \frac{2}{5-3q}, \quad (4)$$

$$\epsilon(\delta v) = \frac{1}{2}(\delta v)^2 + [\delta v - \frac{1}{3}(\delta v)^3]\varphi + \text{HOT}. \quad (5)$$

Here the so-called energy  $\epsilon(\delta v)$  depends on the velocity difference squared plus a correction term proportional to the parameter  $\varphi$ , discussed below;  $\beta$  describes the temperature in the nonequilibrium sense (where  $\beta = 1/k_b T$  for an equilibrium system);  $Z_q$  is the partition function, which is here simply a scaling constant [17]. In our data analysis we examine three possible forms for  $\varphi$ : (a) no correction,

$$\varphi = 0, \quad (6)$$

(b) a form obtained from physical arguments and used in an analysis of Couette–Taylor turbulence [17],

$$\varphi = -0.124(q - 1), \quad (7)$$

and (c) a correction proportional to the skewness  $\xi$ ,

$$\varphi = \frac{1}{2}\xi(q - 1). \quad (8)$$

The skewness is given by

$$\xi = \frac{S_3}{S_2^{3/2}}, \quad (9)$$

with  $S_n(\ell)$  the *structure functions*

$$S_n(\ell) = \langle (\delta v)^n \rangle, \quad (10)$$

which are important quantities in turbulence [22].

The proportionality of  $\varphi$  to  $\xi/2$  in Eq. (8) follows from calculating the skewness from Eqs. (3)–(5), while the proportionality to  $q - 1$  is an assumption guided by the results in Ref. [17]. In the latter reference, yet another form for  $\epsilon(\delta v)$  was used to obtain an improved fit to Couette–Taylor data for  $p(\delta v)$ , but this form introduced another parameter,  $\alpha$ , in addition to  $\varphi$ ; for the present data, Eq. (5) is retained because it provides fits just as well as the modified version of Ref. [17].

Eqs. (3)–(5) give the probability  $p$  for a normalized  $\delta v$  of variance unity, irrespective of the relation between  $\delta v$  and the width of the distribution. Therefore, the measured velocity differences must be normalized by their standard deviation at each  $\ell$  before the fit is performed. The energy correction term  $\varphi$  leads actually to a variance slightly different from unity, but we achieve an average precisely zero and a variance of unity using the renormalized distribution given by  $\tilde{p} = \sigma p(\sigma(\delta v - \langle \delta v \rangle))$ .

## 4. Results

### 4.1. Probability distribution functions

We now fit Eqs. (3)–(5) to our data, examining first the quality of the fits and then the values of  $q(\ell)$  deduced from the data. The form for  $\varphi$  that Beck et al. fitted to data for turbulent Couette–Taylor flow, Eq. (7),

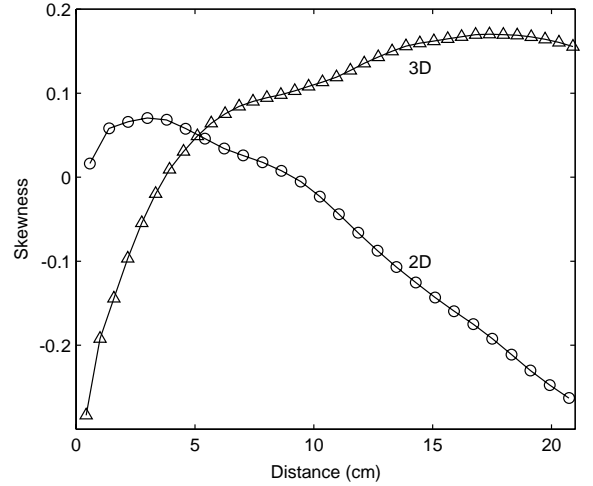


Fig. 3. Skewness of the velocity difference PDF,  $\xi(\ell) = S_3(\ell)/(S_2(\ell))^{2/3}$ , as a function of separation  $\ell$ . The effects of strong shear and rotation lead to a change of the sign of  $S_3$  in both the 2D and 3D cases.

assumes that the skewness  $\xi$  is constant. In 3D turbulence,  $\xi$  is generally small and negative, but for both our 2D and 3D data, we find that  $\xi$  changes sign as a function of distance  $\ell$ , as Fig. 3 illustrates. For homogeneous isotropic turbulence, the sign of  $S_3$  indicates the direction of the energy cascade, which is to large scales in the 2D case and small scales in the 3D case; for our data the dependence of  $\xi$  on  $\ell$  is not understood and will be the subject of future experiments in our laboratory. Given the skewness dependence on  $\ell$ , we examine the fit of the data to Eq. (3) using first Eq. (8) for  $\varphi$ .

Data for  $p(\delta v)$  for both 3D and 2D flows are compared with Eqs. (3)–(5) in Fig. 4. The upper graphs show  $p(\delta v)$  on a linear scale, which emphasizes the fit at the peaks, and the lower graphs show  $p(\delta v)$  on a log scale, which emphasizes the tails of the distribution functions. The data for 2D turbulence fit the predicted  $p(\delta v)$  well over the whole range of length scales. The fits for the 3D flow are also good, even though the functional form for  $p(\delta v)$  changes from one with approximately power law tails for small  $\ell$  to Gaussian for large  $\ell$ . Note that for positive  $\delta v$  for the 3D flow, the theory falls systematically below the data.

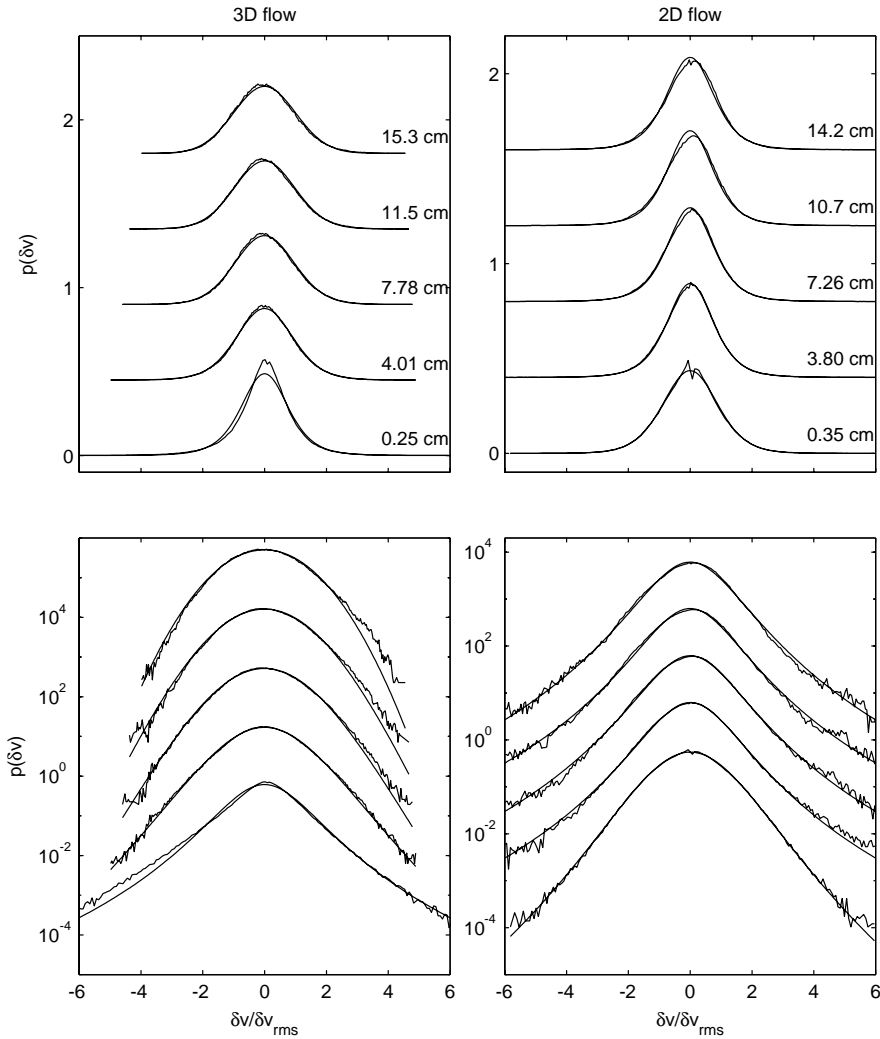


Fig. 4. Comparison of the predicted (smooth curves) and measured velocity difference PDFs for 2D and 3D turbulent flows, plotted on linear axes (top) and log-linear axes (bottom), for measurement points separated by distances  $\ell = 0.3\text{--}15$  cm. The values of the nonextensivity parameter  $q$  deduced from these fits of experiment to theory are shown in Fig. 6.

The goodness of the fit of the measured distribution functions  $p_{\text{exp}}$  to theory  $p_{\text{th}}$  (Eq. (3)) is given by plots of  $(p_{\text{th}} - p_{\text{exp}})/p_{\text{th}}$  as a function of  $\delta v/\delta v_{\text{rms}}$ , as shown in Fig. 5 for all three forms considered for  $\varphi$ . The rms deviations for  $|\delta v| < 2\delta v_{\text{rms}}$  are given in Table 1; we include only two standard deviations in  $\delta v$  because the data for larger  $\delta v$  are noisy and sparse. Surprisingly, the fit with no correction at all,  $\varphi = 0$ , is as good as for the cases using Eq. (7) or Eq. (8); in all cases the difference is typically around 10%.

#### 4.2. Nonextensivity parameter $q$

The values of  $q$  deduced as a function of  $\ell$  from the fits for different forms of  $\varphi$  are presented in Fig. 6. The principal conclusion is that, whatever the form of  $\varphi$ , the nonextensivity parameter  $q$  is approximately constant for the 2D data, independent of  $\ell$ . This indicates that the flow is nonextensive throughout the spatial range examined. Further, the results for  $q$  depend only weakly on the form of the skewness correction  $\varphi$ .

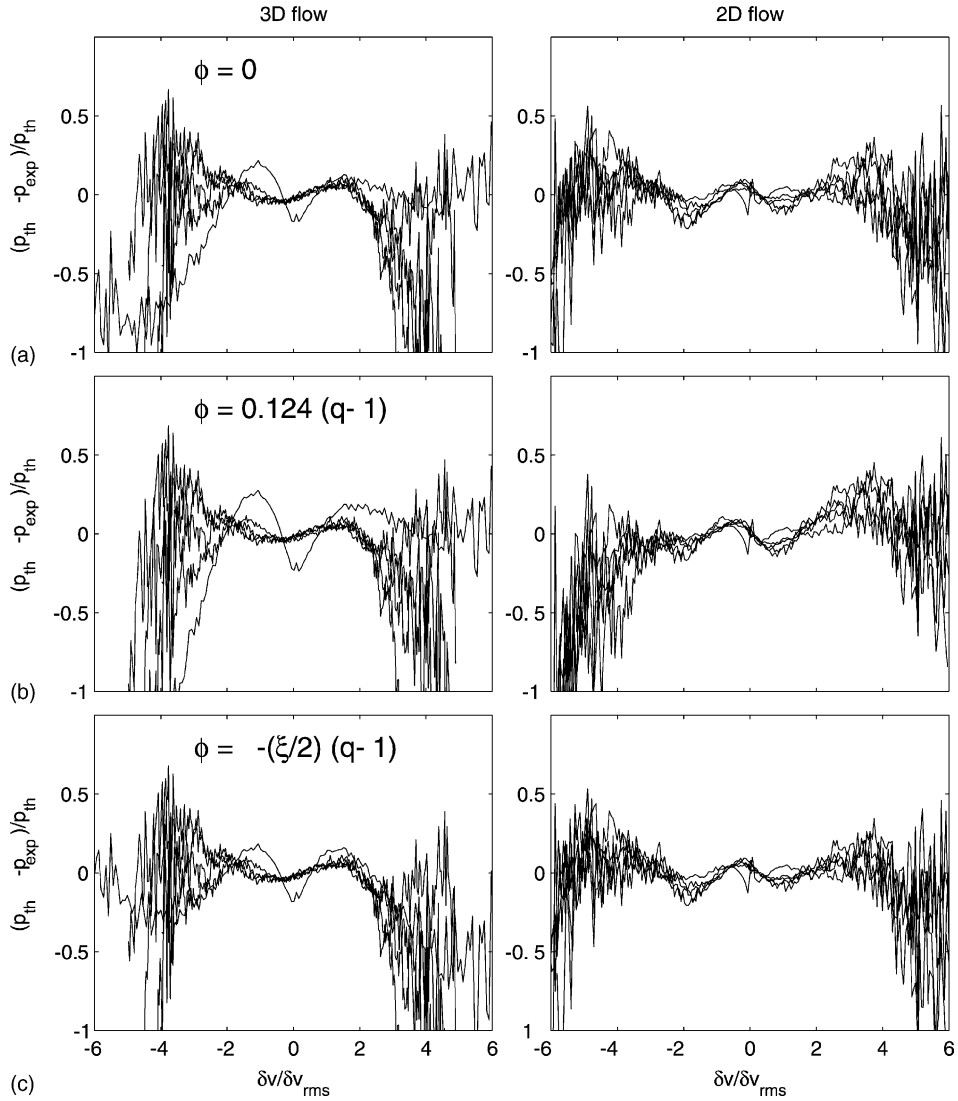


Fig. 5. The difference between theory and experiment for different forms of  $\varphi$  (Eqs. (6)–(8)) for measurement points separated by distances  $\ell = 0.3\text{--}15\text{ cm}$ . The rms differences computed for each case for  $|\delta v| < 2\delta v_{\text{rms}}$  are given in Table 1.

Table 1

Average rms relative difference between theory and experiment for  $|\delta v| < 2\delta v_{\text{rms}}$ , for different values of the distance  $\ell$

	3D separation $\ell$					2D separation $\ell$				
	0.25 cm	4.01 cm	7.78 cm	11.5 cm	15.3 cm	0.35 cm	3.8 cm	7.26 cm	10.7 cm	14.2 cm
$\phi = 0$	0.233	0.082	0.087	0.092	0.108	0.071	0.077	0.106	0.171	0.154
$\phi = -0.124(q-1)$	0.332	0.087	0.076	0.082	0.104	0.075	0.091	0.104	0.152	0.152
$\phi = \xi/2(q-1)$	0.235	0.082	0.083	0.087	0.106	0.071	0.088	0.109	0.164	0.137

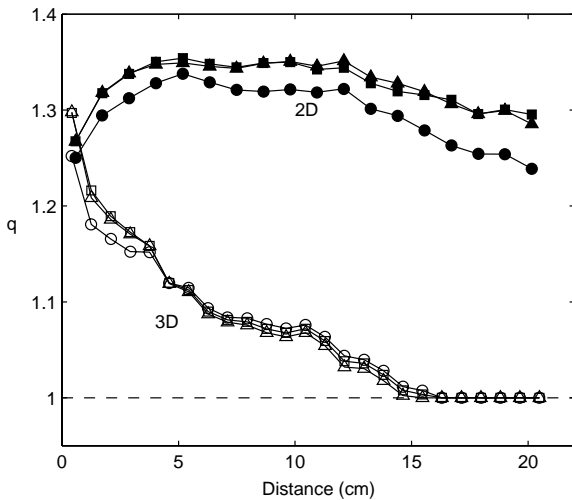


Fig. 6. Nonextensivity parameter  $q$  as a function of separation  $\ell$  for the three forms of the skewness correction:  $\varphi = 0$  (triangles),  $\varphi = -0.124(q - 1)$  (circles), and  $\varphi = \xi(q - 1)/2$  (squares). For 2D turbulence the value of  $q$  is nearly constant, while for the 3D turbulence the value of  $q$  decreases to unity, corresponding to a Gaussian PDF for large  $\ell$  (see Fig. 4).

Given the robustness of the values of  $q$  deduced as a function of  $\ell$  and for different forms of  $\varphi$ , we conclude that  $q_{2D} = 1.32 \pm 0.04$  for our 2D turbulence data.

In contrast to the result for  $q$  for the 2D data, for 3D turbulence we find that  $q$  decreases with increasing  $\ell$  from about 1.25 to unity; again the dependence of  $q$  on the form of  $\varphi$  is very weak. The  $\ell$  dependence is nearly the same as that found for turbulent Couette–Taylor flow [17]: at large  $\ell$ , the flow is extensive ( $q = 1$ ), as expected for 3D turbulence on large scales.

## 5. Discussion

The physical significance of the nonextensivity parameter  $q$  is not well established. A departure from  $q = 1$  may indicate that a flow is intermittent on the scale at which  $q$  was determined. Our earlier analysis of the data for 2D turbulence in terms of the She–Lévêque model [5] yielded a value for the model parameter  $\beta_{SL}$  that indicated a flow dominated by coherent vortices at all scales of the inertial range. The value  $q = 1.32$  that we obtain at all  $\ell$  for the 2D turbulent flow may provide a measure of the extent to

which vortices fill space at all scales. Indeed, numerical simulations [23,24] have shown that coherent vortices cause a strong departure from Gaussian statistics in a turbulent flow.

For the 3D turbulent flow, the value of the She–Lévêque parameter  $\beta_{SL}$  is similar to that for the 2D turbulence, indicating strong intermittency, but we find for 3D turbulence that the nonextensivity parameter decays to unity for large separations  $\ell$ . This is consistent with our observation that the intermittent coherent structures are only present at small scales in the 3D case. It is common for 3D turbulence to display coherent vortices (and hence departures from Gaussianity) at small scales, but these vortices do not grow since no inverse cascade is present. This behavior is captured by the trend in  $q$ , and a large difference between the value for large and small scales indicates a flow which is strongly scale-dependent.

We conjecture that the subsystems which are nonadditive are the coherent vortices and the “sea” of background turbulence in which they exist. In the 3D (slow rotation) case, these vortices only exist at small scales, and therefore  $q$  tends to unity at large scales. In the 2D (fast rotation) case, the coherent vortices can reach large scales, thus creating long range correlations which drive the system into a nonextensive regime.

Finally, the values of  $q$  may give insight about the nature of the turbulent transport. It was found in Ref. [25] that the value of  $q$ , coupled with the dimensionality of the system, can be related to the strength of material transport in a physical system. Furthermore, our 2D flow with strong vortices and a counter-rotating jet may exhibit anomalous (Lévy-type) diffusion, as found in previous experiments on a co-rotating jet at lower Reynolds number [26], and also found in a recent analysis of ocean data [27]. In these quasi-2D flows, particles can become trapped for long times in a vortex and make occasional long excursions (Lévy flights) in a jet, thus enhancing the mixing in the system.

## Acknowledgements

We thank Christian Beck for helpful discussions and Sunghwan Jung for help in the analysis. This

research was supported by the Office of Naval Research.

## References

- [1] R. Kraichnan, Inertial ranges in two-dimensional turbulence, *Phys. Fluids* 10 (7) (1967) 1417–1423.
- [2] J. Sommeria, Experimental study of the two-dimensional inverse energy cascade in a square box, *J. Fluid Mech.* 170 (1986) 139–168.
- [3] J. Paret, P. Tabeling, Experimental observation of the two-dimensional inverse energy cascade, *Phys. Rev. Lett.* 79 (1997) 4162–4165.
- [4] C. Baroud, B. Plapp, Z.-S. She, H.L. Swinney, Anomalous self similarity in a turbulent rapidly rotating fluid, *Phys. Rev. Lett.* 88 (2002) 114501/1–114501/4.
- [5] C.N. Baroud, B.B. Plapp, H.L. Swinney, Z.-S. She, Scaling in three-dimensional and quasi-two-dimensional rotating turbulent flows, *Phys. Fluids* 15 (2003) 2091–2104.
- [6] M. Ragwitz, C. Baroud, B. Plapp, H.L. Swinney, Nonlinear determinism in time series measurements of 2-dimensional turbulence, *Physica D* 162 (2002) 244–255.
- [7] K. Sreenivasan, Fluid turbulence, *Rev. Mod. Phys.* 71 (1999) 383–395.
- [8] B. Castaing, et al., Scaling of hard thermal turbulence in Rayleigh–Bénard convection, *J. Fluid Mech.* 204 (1989) 1–30.
- [9] E.S.C. Ching, Probabilities for temperature differences in Rayleigh–Bénard convection, *Phys. Rev. A* 44 (1991) 3622–3629.
- [10] S.T. Thoroddsen, C.W. van Atta, Exponential tails and skewness of density-gradient probability density functions in stably stratified turbulence, *J. Fluid Mech.* 244 (1992) 547–566.
- [11] B. Shraiman, E.D. Siggia, Lagrangian path integrals and fluctuations in random flow, *Phys. Rev. E* 49 (1994) 2912–2927.
- [12] M. Chertkov, Instanton for random advection, *Phys. Rev. E* 55 (1997) 2722–2733.
- [13] D.T. Son, Turbulent decay of a passive scalar in the Batchelor limit: exact results from a quantum mechanical perspective, *Phys. Rev. E* 59 (1999) R3811–R3814.
- [14] J.C. Bronski, R.M. McLaughlin, Rigorous estimates of the tails of the probability distribution function for the random linear shear model, *J. Stat. Phys.* 98 (2000) 897–915.
- [15] C. Beck, Application of generalized thermostatics to fully developed turbulence, *Physica A* 277 (2000) 115–123.
- [16] C. Tsallis, Possible generalization of Boltzmann–Gibbs statistics, *J. Stat. Phys.* 52 (1988) 479.
- [17] C. Beck, G. Lewis, H.L. Swinney, Measuring nonextensivity parameters in a turbulent Couette–Taylor flow, *Phys. Rev. E* 63 (1999) 035303/1–035303/4.
- [18] C. Beck, On the small-scale statistics of lagrangian turbulence, *Phys. Lett. A* 287 (2001) 240.
- [19] T.H. Solomon, J. Holloway, H.L. Swinney, Shear flow instabilities and Rossby waves in barotropic flow in a rotating annulus, *Phys. Fluids* 5 (1993) 1971–1982.
- [20] J. Sommeria, S. Meyers, H.L. Swinney, Laboratory model of a planetary eastward jet, *Nature* 337 (1989) 58–61.
- [21] R. Mendes, C. Tsallis, Renormalization group approach to nonextensive statistical mechanics, *Phys. Lett. A* 285 (2001) 273–278.
- [22] U. Frisch, *Turbulence: The Legacy of A.N. Kolmogorov*, Cambridge University Press, Cambridge, 1995.
- [23] Z.-S. She, E. Jackson, S. Orszag, Structure and dynamics of homogeneous turbulence: models and simulations, *Proc. R. Soc. London, Ser. A* 434 (1991) 101.
- [24] M. Farge, K. Schneider, N. Kevlahan, Non-Gaussianity and coherent vortex simulation for two-dimensional turbulence using an adaptive orthogonal wavelet basis, *Phys. Fluids* 11 (1999) 2187–2201.
- [25] C. Tsallis, A. de Souza, R. Maynard, Derivation of Lévy-type anomalous superdiffusion from generalized statistical mechanics, in: M. Schlesinger, G. Zaslavsky, U. Frisch (Eds.), *Lévy Flights and Related Topics in Physics*, Springer, Berlin, 1995, pp. 269–289.
- [26] T. Solomon, E. Weeks, H.L. Swinney, Observation of anomalous diffusion and Lévy flights in a two-dimensional rotating flow, *Phys. Rev. Lett.* 71 (1993) 3975–3978.
- [27] A. Reynolds, Lagrangian stochastic modeling of anomalous diffusion in two-dimensional turbulence, *Phys. Fluids* 14 (4) (2002) 1442–1449.